International Journal of Computational and Experimental Science and ENgineering (IJCESEN)

Vol.10 -No.1 (2024) pp. 33-41
http://www.ijcesen.com

ISSN: 2149-9144

Research Article

Study of an Efficient and Environmentally Friendly Germanium-Based $CsGeI_3$ Perovskite Structure For Single and Double Solar Cells

Hayat ARBOUZ*
University Saad Dahlab Blida1, Faculty of Sciences, Department of Physics, 09000, Blida-Algeria
* **Corresponding Author Email:** arbouzhayet@yahoo.fr - **ORCID:** 0000-0003-2780-5215

Article Info:

DOI: 10.22399/ijcesen.250
Received : 10 December 2023
Accepted : 14 February 2024

Keywords

Solar Cell
Tandem
Perovskite
Lead-Free
Optimization

Abstract:

This work deals with the simulation and optimization of a single perovskite solar cell based on the lead-free, inorganic perovskite absorber $CsGeI_3$ with a bandgap energy of 1.6 eV. An appropriate simulation model was designed on the basis of the physical properties employed and carefully selected. Firstly, the study demonstrated the role of increasing the bulk defect density of the absorber as well as the interface defect density at the boundaries between the absorber and the carrier transport layers on increasing the photo-generated carrier recombination velocity, causing the collapse of the solar cell performance. The effect of layer thickness on photovoltaic parameters was also investigated. Next, various combinations of ETL and HTL electron and hole transport materials, with different bandgap alignments with the absorber were studied. The performance of the different structures was used to determine the optimum structure for obtaining the best results. An efficiency of 15.9% was obtained with the ETL-SnO_2 /$CsGeI_3$/HTL- $SrCu_2O_2$ architecture. Finally, the optimized structure was simulated in a 2T-tandem configuration in combination with the 1.3 eV-$CsSnI_3$ based solar sub-cell. It was found that the efficiency could reach 25%. The aim of this work is to develop an efficient, lead-free and stable perovskite cell structure that could replace its hybrid perovskite counterpart and be used as a performing sub-cell in a tandem structure.

1. Introduction

The considerable progress made in harnessing photovoltaic solar energy has led to the development of various systems and devices aimed at performance while remaining inexpensive and easy to manufacture [1]. The emergence of perovskite materials and their application in photovoltaic technology represents a real breakthrough in this field [2]. In recent years, organometallic hybrid perovskite has been the most widely used absorber material in photovoltaic solar cells, due to its advantageous properties that have enabled high conversion efficiencies to be achieved within a decade [3].

The most known halogenated organometallic perovskite is $MAPbI_3$ expressed with the formula ABX_3, where A is a monovalent cation of methylamonium (MA) of chemical formula $CH3NH^{3+}$, B site is a bivalent cation of lead Pb^{+2} , X is a halide anion of the iodine. However, because of the sensitivity of (MA) to temperature and moisture, Formamidinium (FA) of general formula $CH3(NH2)^{2+}$, is favoured in the A site for a better stability. It was also reported that FA-based PSCs was significantly higher than that of MA-based PSCs (25.38 $mAcm^{-2}$ versus 23.26 mA cm^{-2}) [4]. However, perovskite technology has a number of drawbacks that limit its competitiveness compared with older and more mature technologies, such as lead toxicity and the instability of organic components [5]. As a result, the study of inorganic and non-toxic perovskite materials has intensified. Previous work has shown that incorporating inorganic alkali cations such as Cs^+, Rb^+ and K^+ into the (A) site increases the stability and conversion efficiency of solar cells [6].

On the other hand the harmful lead Pb^{2+} can be replaced by other metal ions with low or no toxicity, such as equivalent Sn^{2+} , $Ge^{2+,}$ Bi^{3+} , Sb^{3+}[7]. Replacing Lead with other elements could change the general formula of the perovskite. One speaks sometimes of double perovskites when Pb^{+2} is substituted with one trivalent B^{3+} and one monovalent B^+ resulting in the formula $A_2B'B''X_6$.

The perovskite that is the subject of this study is $CsGeI_3$, where inorganic caesium (Cs) occupies site (A) and lead has been replaced by its equivalent Ge^{+2} because of its very low toxicity [8]. However, it should not be forgotten that Ge^{+2} shares with Sn^{2+} a strong tendency to oxidize at room temperature. Fortunately, a number of methods exist to overcome this problem [9]. Germanium-based perovskite thin films have been the subject of much experimental and computational research.

This work concerns the simulation and optimization of a single solar cell based on the inorganic, lead-free absorber $CsGeI_3$, followed by a study of the performance of a tandem solar cell based on the same structure as a top sub-cell. The aim is to obtain high-performance structures that could contribute to the development of efficient solar cell devices based on low-cost, non-toxic and stable perovskite absorbers.

2. Structure, Methodology and Theoretical Model

The simulation work was carried out on the basic structure, which has a conventional architecture of successive layers configured as follows [10]: FTO/PCBM/$CsGeI_3$/Spiro-OMeTAD/Ag. The absorbing perovskite layer is inorganic, lead-free $CsGeI_3$, with a bandgap energy of 1.6 eV and a thickness of 1 µm. The materials for the initial ETL and HTL layers were PCBM and Spiro-OMeTAD, measuring 50 nm and 200 nm respectively. FTO was used as the transparent oxide layer and Ag as the back contact.

The study begins by examining the effect of the bulk defect density of the perovskite absorber in addition to that of the interface defect density on the carrier recombination and photovoltaic performance of the device. The impact of varying the thickness of the main layers mentioned above was then simulated.

The results obtained suggested optimum values for these parameters.

Next, different combinations of ETL and HTL materials, which produce different bandgap alignments at the interfaces with the absorber material, were studied. The performance of the different structures was calculated in order to select the optimum configuration that gives the best photovoltaic performance.

To conclude this study, the performance of the two-terminal tandem solar cell was simulated. The optimal $CsGeI_3$ cell occupies the position of the top sub-cell in combination with the perovskite-based $CsSnI_3$ solar cell with lower bandgap energy as the bottom sub-cell. The results obtained were compared with those of similar work.

The simulation model used in this work consists of calculating the photocurrent density, the current-voltage characteristic and the photovoltaic parameters on the basis of equations derived from the solution of the Poisson equation and the drift-diffusion equations for electrons and holes [11].

$$J_{ph} = q \int_{\lambda_{min}}^{\lambda_{max}} F(\lambda).EQE(\lambda)\, d\lambda \qquad (1)$$

J_{ph} is the photocurrent density which depends on the external quantum efficiency EQE (λ) and the incident solar spectrum F(λ). q is the electron's elementary charge. λ_{min} and λ_{max} are the minimum and maximum wavelengths.

The current-voltage characteristic is expressed in equation 2.

$$J(V) = J_{ph} - (J_0 + J_s).\left(e^{\frac{q.(V-JR_S)}{2kT}} - 1\right) - \frac{V-J.R_S}{R_{sh}} \qquad (2)$$

The recombination rate due to the density of defects in the bulk of the perovskite material was evaluated according to the Schockley-Read-Hall recombination model [12], expressed in equation 3.

$$R_{SRH} = \frac{n.p-n_i^2}{\tau_p.(n+n_i)+\tau_p.(p+p_i)} \qquad (3)$$

n and p represent the concentrations of electrons and holes. τ_n and τ_p are electron and hole life-times given by equation 4.

$$\tau_{n,p} = \frac{1}{\sigma_{n,p}.V_{th}.N_t} \qquad (4)$$

N_t is the bulk defect density in the perovskite material and V_{th} is the thermal velocity.

The effect of interface density at the vicinity of the absorber with its neighbouring ETL electron transport and HTL hole transport layers, was investigated in this work. The contribution of interface recombination at the rear and the front interfaces on each side of the perovskite absorber, was taken into consideration in the evaluation of the current-voltage curve [13]. J_s represent in equation 2, the current loss due to interface recombination which depends on the recombination velocity S and the bandgap energy offsets ΔE_c and ΔE_v at both sides of the perovskite absorber. Equations 5, 6 and 7 express S, ΔE_c and ΔE_v.

$$S = V_{th}.\sigma.N_{int} \qquad (5)$$

N_{int} is the interfacial defect density and σ is the capture

cross section of traps.

$$\Delta E_c = \chi_{ETL} - \chi_{Abs} \quad (6)$$

$$\Delta E_v = (\chi_{HTL} + Eg_{HTL}) - (\chi_{Abs} + Eg_{Abs}) \quad (7)$$

The basic physical parameters used in this simulation have been taken from research works on the materials used in the structure [14,15,16,17].

3. Result and Discussion

3.1 Effect of Bulk Defect Density N_t

Although the nature of defects in hybrid and inorganic perovskites remains poorly understood and is still under investigation, studies have demonstrated a direct relationship between the density of traps in the body of the perovskite and the collection rate [18,19].
The relationship between increasing defect density in $CsGeI_3$ perovskite and the photovoltaic parameters of the $CsGeI_3$-based solar cell was simulated using the established model, where the recombination rate was evaluated using the Shockley-Read-Hall approach. The curves are shown in Fig. 1, when the N_t defect density of the absorbing perovskite layer varies 10^{12} cm^{-3} to $10^{22}cm^{-3}$.

Between 10^{12} cm^{-3} and $10^{15}cm^{-3}$, the curves show a slight decrease in photo-current density from 18.93 mA/cm² to 18.52 mA/cm², stability of open-circuit voltage at 0.88 and form factor at 78%, and a decrease in conversion efficiency from 13.86% to 13.57%. This can be interpreted as a stability of PV parameters over this defect density range. On the other hand, there is a real degradation of the PV parameters beyond $10^{15}cm^{-3}$, except for FF, which increases slightly.

3.2 Impact of Defect Density N_{int} at ETL/CsGeI3 and CsGeI3/HTL interfaces

The perovskite surface in PSCs is covered with an electron transport layer ETL and a hole transport layer HTL on both sides, forming interfaces that are the site of spurious recombination due to the presence of trap defects. This effect has been explored in this section, by observing the effect of increasing the defect density at the PCBM/$CsGeI_3$ and $CsGeI_3$/Spiro-OMeTAD interfaces on the photovoltaic parameters of the device studied**.** The results are depicted in Fig. 2. The influence of the defect density on the device performance is broadly similar to that of the bulk defect density in the absorber studied above, i.e. some stability of the photovoltaic parameters is observed when the defect density is below 10^{14} cm^{-3}, but most of these parameters drop beyond this value. Photocurrent density appears to be insensitive to increasing defect density at the PVK/HTL interface. On the other hand, the conversion efficiency, which is also subject to the explained effect, is more affected by the increase in defect density at the ETL/PVK interface than by that behind the PVK/HTL interface, as shown in Fig.2 (d).

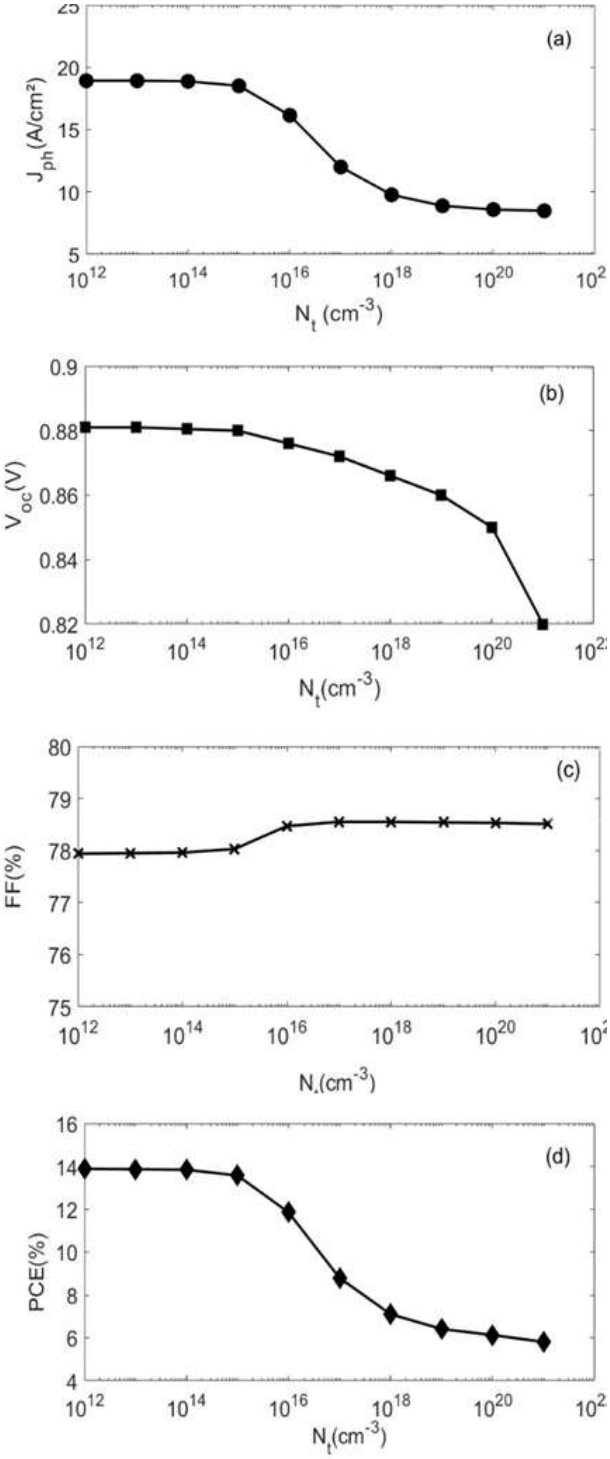

Figure 1. *Impact of the Bulk Defect Density on the PV parameters of the $CsGeI_3$-based PSC.*

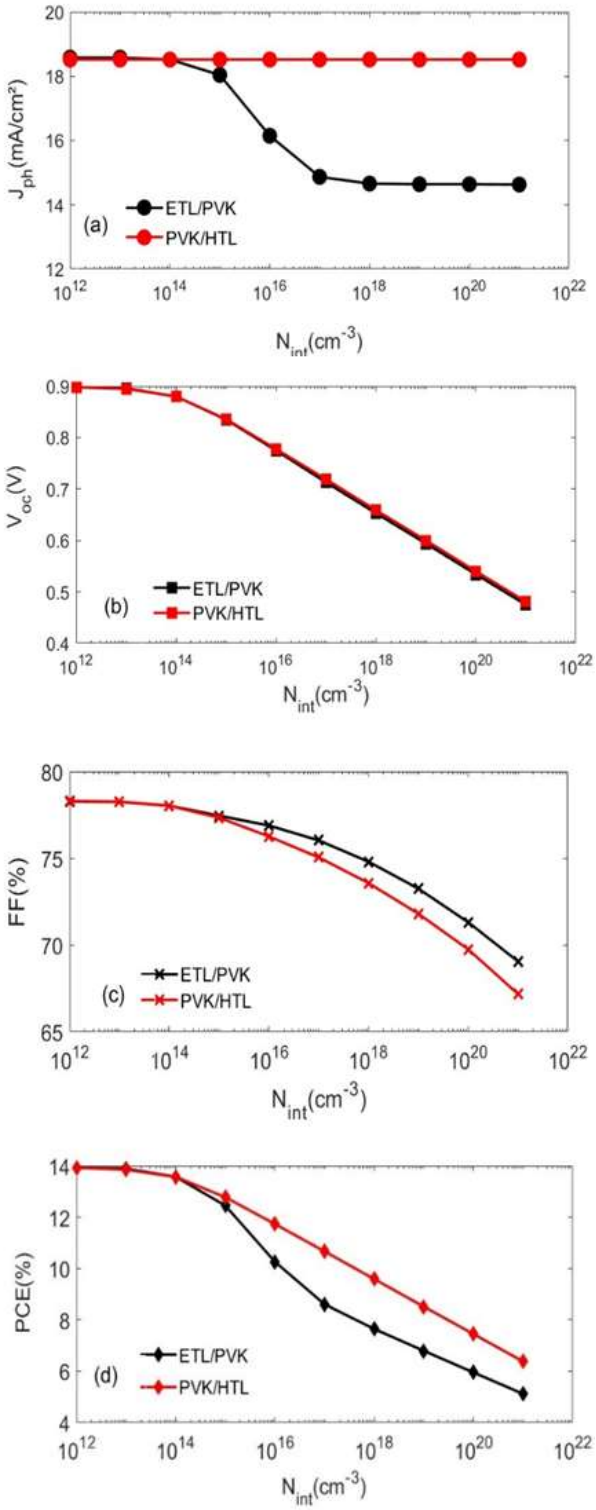

Figure 2. *Impact of the Bulk Defect Density on the PV parameters of the $CsGeI_3$-based PSC.*

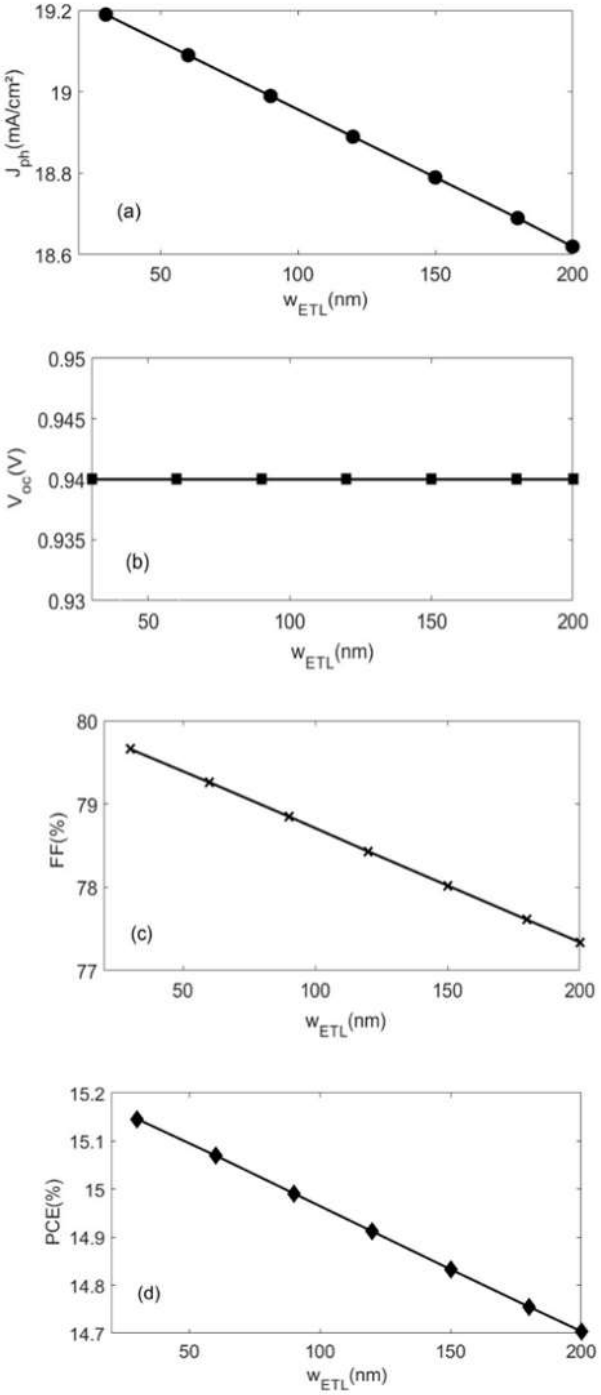

Figure 3. *Impact of the PCBM-ETL thickness on the PV parameters of the $CsGeI_3$-based PSC.*

3.3 Impact of ETL and HTL thickness

Like the thickness of the perovskite absorber, the thickness of the carrier transport layers also influences the photovoltaic parameters of the solar cell and must therefore be optimised to obtain optimum performance.

Fig.3 and Fig.4 show the variation in photovoltaic parameters as a function of ETL and HTL material thickness.

The decrease in all PV parameters can be seen in Fig.3 (a), (b), (c) and (d), as the thickness of the ETL PCBM increases due to the increase in parasitic absorption that occurs in this layer as its thickness increases and causes a reduction in the photocurrent density of the electrons. This means that it is recommended to use the thinnest thickness for this

layer, but thick enough to cover the absorber, as was observed in the experiment [20].

Fig.4. shows the effect of augmenting the Spiro-OMeTAD-HTL thickness on the PV performance of the simulated solar cell.

The augmentation of all parameters is shown when the thickness is varied from 50nm to 500 nm.

The transport layers play an essential role in PSCs and have a significant impact on the device's performance. The function of the electron transport layer is to promote the extraction and transport of electrons from the absorber to the front electrode and to block the passage of holes, while the role of the hole transport layer HTL is to promote the extraction of holes and to block the passage of electrons to the rear electrode [21]. A favourable alignment of the conductive and valence bands on either side of the perovskite layer is recommended, as well as appropriate photoelectric properties that favour carrier extraction and transport.

3.4 Performance of Alternatives ETLs-based Structures

PCBM has been widely used as an electron transport layer material in PSCs due to its ease of deposition and excellent electron mobility, which enables high conversion efficiencies to be achieved. However, it has been reported that PCBM does not cover the rough surface of the perovskite absorber as well as other electron transport materials and its organic nature favours instability [22], hence the need to study inorganic materials as electron transport layers. In this study, several materials were proposed to replace the PCBM of the basic structure. These are SnO_2, TiO_2, IGZO and ZnSO. The performance of the structures based on these materials are presented in table 1.

The results obtained with the ETLs of TiO_2 and IGZO are very similar to those of the basic structure. The difference lies in the value of the CBO conduction band offset, which is higher between $CsGeI_3$ and IGZO. On the other hand, the structure with ZnSO-ETL gave poorer performance than the base structure, although the CBO was close to alignment. The structure based on the SnO_2 electron transport

Table 1. *Performance of ETL-based structures*

ETL	J_{ph} mA/cm²	V_{oc} Volts	FF %	PCE %	ΔE_c eV
PCBM	20.08	0.941	78.5	15.83	0.38
SnO_2	20.07	0.947	78.8	15.94	0.48
TiO_2	20.08	0.940	78.3	15.84	0.38
IGZO	20.08	0.931	78.4	15.80	0.64
ZnOS	20.07	0.942	78.3	15.62	0.08

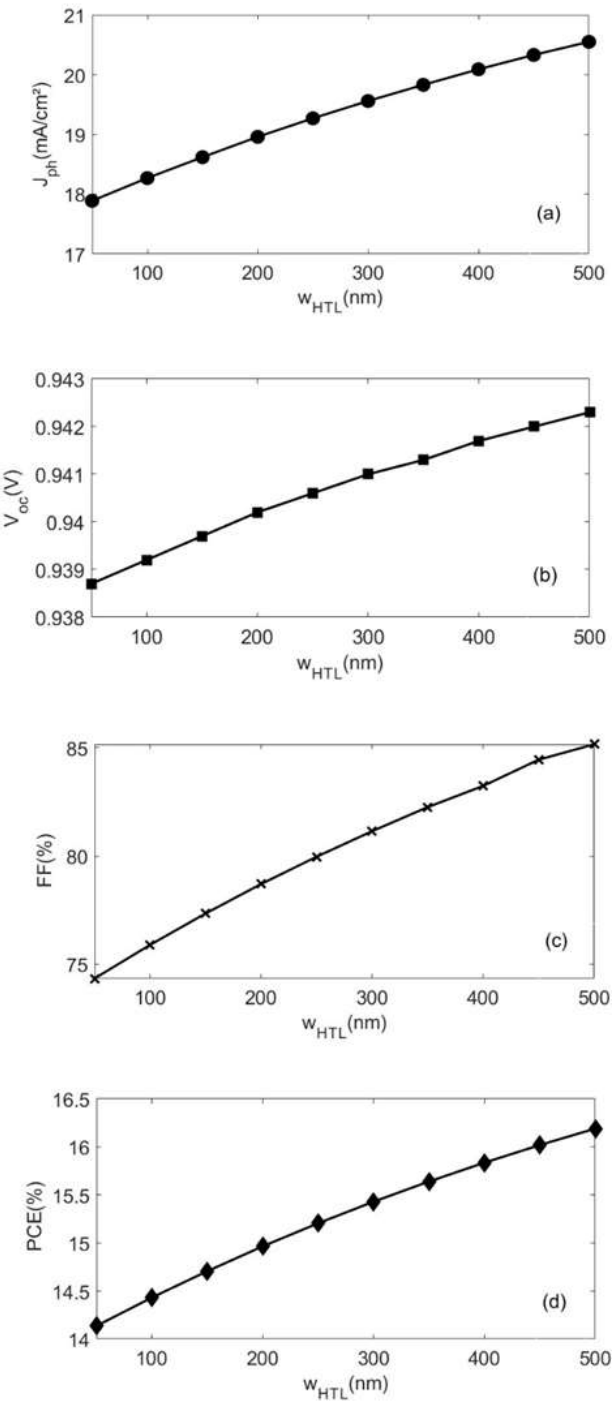

Figure 4. *Impact of the Spiro-OMeTAD-HTL thickness on the PV parameters of the $CsGeI_3$-based PSC*

layer recorded the best performance, and was therefore considered the most favourable candidate for replacing the PCBM material in the device, despite its higher CBO than that of the base structure.

3.5 Performance of Alternatives HTLs-based Structures

Spiro-OmeTAD HTM is commonly used in high-performance PSCs [23] due to its high performance potential and ease of low-temperature processing.

However, its low hole mobility and high cost mean that it can be replaced by HTLs that do not have these problems, such as inorganic copper-based materials Cu_2O, CuI and $SrCu_2O_2$, as well as Ni-based materials such as NiO [14], which were investigated in this letter. The performance of their corresponding structures are grouped in table 2. The results showed inferior performance to the baseline structure for Cu_2O and CuI HTLs, while NiO and $SrCu_2O_2$ based structures recorded similar performance.

However, $SrCu_2O_2$ was preferred due to the alignment of the valence band with that of the $CsGeI_3$ perovskite absorber.

4. Optimization and Performance

Based on these results, we considered the following optimum structure: FTO/SnO_2/$CsGeI_3$/$SrCu_2O_2$/Ag, where SnO_2 and $SrCu_2O_2$ materials with respective thicknesses of 50 nm and 350 nm were determined as alternatives to the PCBM and Spiro-OMeTAD layers of the basic device. The thickness and defect density of the $CsGeI_3$ absorber layer were set at 1µm and $10^{14}cm^{-3}$ respectively, while the defect density at the interfaces adjacent to the transport layers was set at $10^{13}cm^{-3}$. The J-V curve of the optimised device is shown in Fig. 5 and compared with that of the basic structure. The corresponding photovoltaic performance is shown in table.3.

Table 2. *Performance of HTL-based structures*

HTL	J_{ph} mA/cm²	V_{oc} Volts	FF %	PCE %	ΔE_v eV
Spiro-OMeTAD	20.08	0.941	78.5	15.83	0.23
Cu_2O	18.12	0.939	78.9	14.31	0.27
CuI	19.88	0.941	78.5	15.63	0.20
$SrCu_2O_2$	20.07	0.941	78.5	15.83	0.01
NiO	20.07	0.941	78.5	15.82	0.30

Table 3. *Optimal Performance*

Basic: FTO/PCBM/$CsGeI_3$/Spiro-OMeTAD/Ag					
J_{ph} mA/cm²	V_{oc} Volts	FF %	PCE %	ΔE_c eV	ΔE_v eV
20.08	0.941	78.50	15.83	0.38	0.30
Optimal: FTO/SnO_2/$CsGeI_3$/$SrCu_2O_2$ /Ag					
J_{ph} mA/cm²	V_{oc} Volts	FF %	PCE %	ΔE_c eV	ΔE_v eV
20.07	0.948	78.6	15.93	0.48	0.01

5. 2T-tandem Structure based on $CsGeI_3$

Conversion efficiency can be further improved by designing new device structures such as tandem solar cells that are capable of achieving a PCE exceeding the Shockley-Queisser limit of single-junction solar cells thanks to a wider exploitation of the solar spectrum.

The exceptional properties of perovskites offer great potential for their use in tandem devices. The final part of the study consists of simulating the above optimized $CsGeI_3$ solar cell structure as the top cell of a tandem structure, combined with a bottom cell based on $CsSnI_3$ perovskite with a lower bandgap energy of 1.3 eV, which has already been optimized in a previous work.

The monolithically integrated two-terminal 2-T architecture was considered, where the two parts are connected in series, so the voltages generated by the two sub-cells are summed, but their photo-generated currents must be matched [24]. Otherwise, the overall photocurrent of the tandem will be limited to that of the sub-cell generating the smallest current.

Fig.6 illustrates the current matching condition that allows the upper and lower sub-cells to have the same J_{SC} values. This was achieved by thinning the $CsGeI_3$ absorber layer of the upper sub-cell.

The current was found to correspond to a thickness of 380 nm where both photocurrents are equal to 14.91 mA/cm².

An efficiency of 24.9% was obtained, the voltage was increased to 1.74 V and the fill factor to 85%.

The J-V curves for the top, bottom and tandem cells are shown in Fig.7. The PCE of the tandem device was calculated and listed in table 4 along with that of other tandem devices reported in the literature for comparison. The efficiency obtained by the simulated tandem device is very close to that of reference [25] which has a bottom silicon heterojunction and also to that of reference [26] based on the Bottom 1.22 eV- perovskite of $MAFAPbSnI_3$.

However, this study recorded a better PCE than the 1.25 eV poly-silicon/SiO_2, 1.25 eV c-Si and 1.25 eV CIGS based structures of references [27,28,29]. In general, a good correlation was found with the reported results.

5. Conclusion

A Single perovskite solar cell based on the absorbing perovskite material $CsGeI_3$ with a bandgap energy of 1.6 eV was the subject of this work. This perovskite is inorganic, lead-free and easy to fabricate. The study began by examining the effect of the density of defects in the overall absorber and at the interfaces between the perovskite and its neighbouring ETL and HTL layers, and of the thickness of these layers, on the photovoltaic parameters of the solar cell. A model for calculating the J-V curve has been described

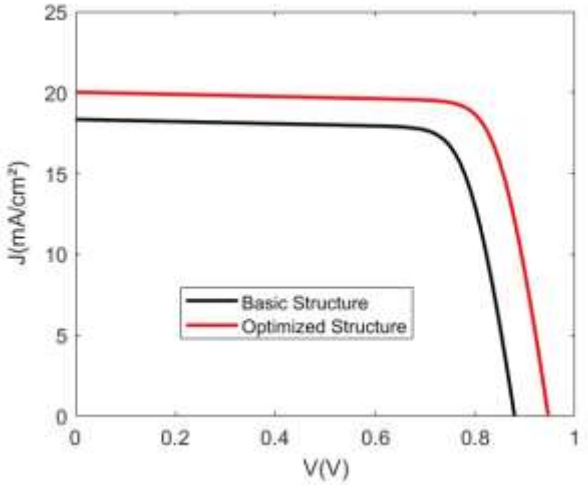

Figure 5. *J-V characteristic of the $CsGeI_3$-based device.*

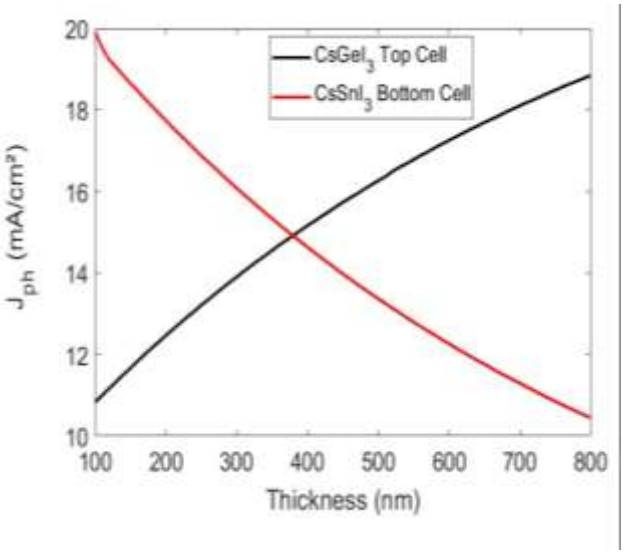

Figure 6. *Current Matching Condition in 2-T $CsGeI_3$/$CsSnI_3$ Tandem SC.*

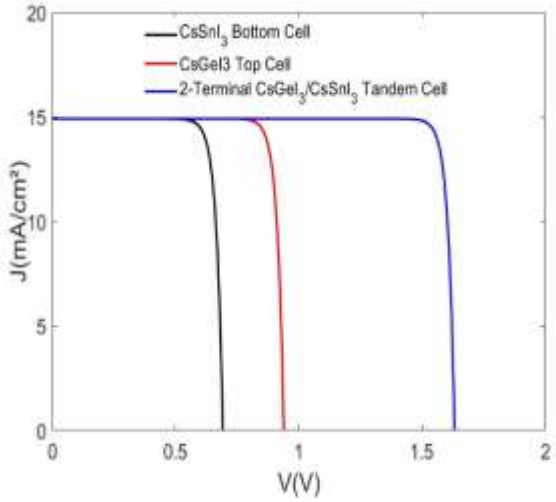

Figure 7. *J-V curve of (2-T) $CsGeI_3$/$CsSnI_3$ Tandem SC*

Table 4. *Performance of PVK Tandem Devices*

Top PSC / E_g(eV)	**Bottom PSC / E_g(eV)**	**PCE (%)**
$CsGeI_3$/ 1.6	$CsSnI_3$/ 1.3	24.9 This work
CsFaPb(IBr)3/ 1.6	Si-HJ 1.25	25.2 [25]
$CsRbFAMAPb(IBr)_3$/ 1.63	Poly-Si/SiO_2 /1.22	24.2 [26]
$CsRbFAMAPb(IBr)_3$/ 1.62	Homo-c-Si/ 1.25	22.5 [27]
$CsMAFAPb(IBr)_3$/ 1.63	CIGS/ 1.25	23.1 [28]
CsFaPb(Ibr)3 /1.77	$MAFAPbSnI_3$/ 1.22	24.8 [29]

in which the effect of bandgap energy offsets at the interfaces has been taken into account. The performance of structures based on alternative materials of the ETL and HTL layers was simulated, and the results obtained were compared with those of the basic structure, depending on their photovoltaic performance and their appropriate band alignment with the $CsGeI_3$ absorber. According to the simulation results obtained, the SnO_2/$CsGeI_3$/ $SrCu_2O_2$ configured structure was favoured as the optimal structure, for which an improved efficiency of 15.93% was achieved. Finally, the structure was simulated as the top subcell in a tandem configuration with the bottom subcell of $CsSnI_3$ that was the subject of previous work. The efficiency was increased to 24.9%. The results correlate well with some of the reported results.

The aim of this project is to develop technology based on lead-free, stable and inorganic perovskites in a single and tandem architectures.

Author Statements:

- **Ethical approval:** The conducted research is not related to either human or animal use.
- **Conflict of interest:** The authors declare that they have no known competing financial interests or personal relationships that could have appeared to influence the work reported in this paper
- **Acknowledgement:** The authors declare that they have nobody or no-company to acknowledge.
- **Author contributions:** The authors declare that they have equal right on this paper.
- **Funding information:** The authors declare that there is no funding to be acknowledged.
- **Data availability statement:** The data that support the findings of this study are available on request from the corresponding author. The data

are not publicly available due to privacy or ethical restrictions.

References

[1] Nikolaidis P. (2023). Solar Energy Harnessing Technologies towards De-Carbonization: A Systematic Review of Processes and Systems. *Energies*.16(17):6153. https://doi.org/10.3390/en16176153

[2] Wang, F., Ge, C., Duan, D., Lin, H., Li, L., Naumov, P. and Hu, H. (2022), Recent Progress in Ionic Liquids for Stability Engineering of Perovskite Solar Cells. *Small Struct.*, 3: 2200048.https://doi.org/10.1002/sstr.202200048

[3] A. Hossain, P. Bandyopadhyay, A. Karmakar, A.K.M. Atique Ullah, R. K. Manavalan, K. Sakthipandi, N. Alhokbany, S. M. Alshehri, J. Ahmed (2022). The hybrid halide perovskite: Synthesis strategies, fabrications, and modern applications,*Ceramics International*, 48(6); 7325-7343

[4] Liu, S., Biju, V.P., Qi, Y. *et al.* (2023). Recent progress in the development of high-efficiency inverted perovskite solar cells. *NPG Asia Mater* **15**;27. https://doi.org/10.1038/s41427-023-00474-z

[5] K Rao, Maithili & D N, Sangeetha & Kumar, Selva & Y N, Sudhakar & M G, Mahesha. (2021). Review on persistent challenges of perovskite solar cells' stability. *Solar Energy*. 218. 469-491. 10.1016/j.solener.2021.03.005.

[6] Q. Wali, F.J. Iftikhar, M. Ejaz Khan, A. Ullah, Y. Iqbal, R. Jose, (2020). Advances in stability of perovskite solar cells, *Organic Electronics*, 78;105590, https://doi.org/10.1016/j.orgel.2019.105590.

[7] Tambwe, K.; Ross, N.; Baker, P.; Bui, T.-T.; Goubard, F. (2022). Humidity Sensing Applications of Lead-Free Halide Perovskite *Nanomaterials. Materials*, 15;4146. https://doi.org/10.3390/ ma15124146

[8] S. Solanki, K. V. Bharathi, K. Bhargava, (2022). Fundamental analysis of lead-free CsGeI3 perovskite solar cell, *Materials Today: Proceedings*,67(1);180-186, https://doi.org/10.1016/j.matpr.2022.06.182

[9] S. Aina, B. Villacampa, M. Bernechea, (2021) Earth-abundant non-toxic perovskite nanocrystals for solution processed solar cells: *Mater. Adv.*, 2; 4140. DOI: 10.1039/d1ma00245g

[10] I. Chabri, A. Oubelkacem, Y. Benhouria, A. Kaiba, I. Essaoudi, A. Ainane, (2023). Performance optimization of a CsGeI3-based solar device by numerical simulation, *Materials Science and Engineering:* B, 297;116757,https://doi.org/10.1016/j.mseb.2023.116757.

[11] H. Arbouz, (2023). Simulation study of single solar cell structures based on the compositionally variable perovskite material CsSn(I1−xBrx)3 for tandem configured solar cells, *Journal of Engineering Research*, https://doi.org/10.1016/j.jer.2023.09.030.

[12] H. Arbouz, (2023). Towards efficient tandem solar cells based on lead-free and inorganics perovskite absorbers, *Therm. Sci. Eng.* 6 (1);34, https://doi.org/10.24294/ tse.v6i1.2000.

[13] H. Arbouz, (2023). Optimization of lead-free CsSnI3-based perovskite solar cell structure, *Appl. Rheol.* 33(1);20220138, https://doi.org/10.1515/arh-2022-0138

[14] Shasti, M. and Mortezaali, A. (2019), Numerical Study of Cu_2O, $SrCu_2O_2$, and $CuAlO_2$ as Hole-Transport Materials for Application in Perovskite Solar Cells. *Phys. Status Solidi A*, 216: 1900337. https://doi.org/10.1002/pssa.201900337

[15] Ahmad W, Noman M, Tariq Jan S, Khan AD. (2023) Performance analysis and optimization of inverted inorganic CsGeI3 perovskite cells with carbon/copper charge transport materials using SCAPS-1D. R. *Soc. Open Sci.* 10: 221127. https://doi.org/10.1098/rsos.22112

[16] N. Shukla, A. K.. Verma, S. Tiwari, Optimization of Efficient Perovskite-Si Hybrid Tandem Solar Cells, Mat. Sci. Res. India.20 (1).

[17] T.K. Tulk, N. Alam, M. Akhtaruzzaman , K. Sobayel , M. M. Hossain (2022). Optimization of a high-performance lead-free cesium-based inorganic perovskite solar cell through numerical approach, *Heliyon* 8. https://doi.org/10.1016/j.heliyon.2022.e11719

[18] H. Arbouz, (2022). Simulation and Optimization of a Lead-Free CS2TiBr6 Perovskite solar cell structure, *International Conference on Electrical, Computer, Communications and Mechatronics Engineering (ICECCME)*, Maldives, Maldives, 2022;1-6, doi: 10.1109/ICECCME55909.2022.9987837.

[19] H. Arbouz, (2023). Simulation and Optimization of a solar Cell Based on the Double perovskite Absorber Material Cs2BiAgI6, *3rd International Conference on Electrical, Computer, Communications and Mechatronics Engineering (ICECCME)*, Tenerife, Canary Islands, Spain, 2023;1-6, doi: 10.1109/ICECCME57830.2023.10252226.

[20] H. Lu, Y. Ma, B. Gu, W. Tian and L. Li, (2015). Identifying the optimum thickness of electron transport layers for highly efficient perovskite planar solar cells, *J. Mater. Chem. A*, 3, 16445-16452. https://doi.org/10.1039/C5TA03686K

[21] Bhardwaj, Km & Rai, Shambhavi & ., Sadanand & Lohia, Pooja & Dwivedi, D.K.. (2021). Investigating the performance of mixed cation mixed halide-based perovskite solar cells using various hole-transport materials by numerical simulation. *Optical and Quantum Electronics.* 53. 10.1007/s11082-021-03262-7.

[22] P. Patil, D. S. Mann, U. T. Nakate, Y.B Hahn, S.N. Kwon, S.I. Na, (2020). Hybrid interfacial ETL engineering using PCBM-SnS2 for High-Performance p-i-n structured planar perovskite

solar cells,*Chemical Engineering Journal*, 397;125504, https://doi.org/10.1016/j.cej.2020.125504.

[23] Li, S., Cao, YL., Li, WH. *et al.* (2021). A brief review of hole transporting materials commonly used in perovskite solar cells. *Rare Met.* 40, 2712–2729. https://doi.org/10.1007/s12598-020-01691-z

[24] Bailie. C, Christoforo. M, Mailoa. J, Bowring . A, Unger. E, Nguyen. W. et al, (2014). Semi-Transparent Perovskite Solar Cells for Tandems with Silicon and CIGS. *Energy & Environmental Science.* 8. DOI:10.1039/C4EE03322A

[25] Sahli, F.; Werner, J.; Kamino, B. A.; Brauninger, M.; Monnard,¨ R.; Paviet-Salomon, B. et al. (2018). Fully Textured Monolithic Perovskite/Silicon Tandem Solar Cells with 25.2% Power Conversion Efficiency. *Nat. Mater.* 17, 820−826

[26] Lin, R.; Xiao, K.; Qin, Z.; Han, Q.; Zhang, C.; Wei, M. et al. (2019). Monolithic AllPerovskite Tandem Solar Cells with 24.8% Efficiency Exploiting Comproportionation to Suppress Sn(ii) Oxidation in Precursor Ink. *Nat. Energy* 4, 864−873.

[27] Wu, Y.; Yan, D.; Peng, J.; Duong, T.; Wan, Y.; Phang, S. et al. (2017). Monolithic Perovskite/ Silicon-Homojunction Tandem Solar Cell with Over 22% Efficiency. *Energy Environ. Sci.* 10;2472−2479.

[28] Al-Ashouri, A.; Magomedov, A.; Ross, M.; Jost, M.; Talaikis, M.; Chistiakova, G. et al. (2019). Conformal Monolayer Contacts with Lossless Interfaces for Perovskite Single Junction and Monolithic Tandem Solar Cells. *Energy Environ. Sci.* 12; 3356−3369

[29] Shen, H. P.; Omelchenko, S. T.; Jacobs, D. A.; Yalamanchili, S.; Wan, Y. M.; Yan, D. et al. (2018). In Situ Recombination Junction Between P-Si and TiO2 Enables High-Efficiency Monolithic Perovskite/Si Tandem Cells. *Sci. Adv*. 4;9711